Accepted version (peer-reviewed preprint) of the paper:

Pérez-Docampo, M., Morillas, L., Balmori-Roiz, J. A., & Escolano-Margarit, D. (2023). GIS Framework for Rapid Seismic Loss Assessment: Case Study of Granada Metropolitan Area. *Journal of Earthquake Engineering*, *27*(7), 1665-1689.

https://doi.org/10.1080/13632469.2022.2086185

https://www.tandfonline.com/doi/abs/10.1080/13632469.2022.2086185

GIS framework for rapid seismic loss assessment: case study of Granada metropolitan area

Manuel Pérez-Docampo[a], Leandro Morillas[a,b]*, José Antonio Balmori-Roiz[c], David Escolano-Margarit[d]

[a]*Department of Structural Mechanics and Hydraulic Engineering. School of Architecture, Universidad de Granada, Spain;*

[b]*Andalusian Institute of Geophysics and Earthquake Disaster Prevention, Universidad de Granada, Spain;*

[c]*Department of Building Construction, Geotechnical Engineering, Continuum Mechanics and Theory of Structures, Universidad de Valladolid, Spain;*

[d]*Department of Mechanical Engineering, Universidad Politécnica de Madrid, Spain.*

*Corresponding author:

Leandro Morillas

Department of Structural Mechanics and Hydraulic Engineering. School of Architecture, Universidad de Granada

Campo del Príncipe, 18071 Granada (Spain)

lmorillas@ugr.es

GIS framework for rapid seismic loss assessment: case study of Granada metropolitan area

Traditional vulnerability methodologies rely on collecting building data through time consuming surveys and visual screening. Geospatial infrastructure systems have rapidly evolved and today we can access massive geospatial data. Digital cadastral databases combine location, attributes, and temporal information for building stock. This paper proposes a GIS-based framework to estimate seismic vulnerability and losses from cadastral data only. The framework is rooted on well-known displacement-based procedures and uses probabilistic models of the building structural capacity. A featured application to 287,503 housing units in metropolitan area of Granada is presented to showcase outputs for decision-making: performance displacement, damage level and repair cost.

Keywords: Geographic Information Systems; Seismic Losses; Vulnerability; Environmental Risks; Decision-Making.

Introduction

The evaluation of the seismic risk in a determined area is always a complex problem since we are dealing with the prediction of future losses given an expected seismic hazard. Losses are a broad concept that include not only physical damage to buildings but also social, economic, and psychological aspects, making the problem very difficult to objectivize. Although complex, it is absolutely necessary in earthquake prone areas to evaluate and understand the risk over a period of time in order to: i) Raise awareness of seismic risk among decision makers and the public; ii) Provide tools to local institutions to make informed decisions; iii) Develop risk mitigation plans; iv) Anticipate the possible nature and scope of the emergency response needed to cope with an earthquake-related disaster and v) Develop plans for recovery and reconstruction following a disaster. In this sense the seismic damage scenarios are a paramount tool to picture the problem. A seismic damage scenario is a mean of characterize and quantify the damage that a specific earthquake can exert and its spatial distribution. The evaluation of risk or losses requires,

on the one hand, an estimation of the seismic hazard in site and, on the other hand, a vulnerability analysis of the building stock exposed.

There are several methodologies proposed for the estimation of seismic damage scenarios. At global level, the United Nations developed the Risk Assessment Tool for Diagnosis of urban areas against seismic disasters RADIUS (UN 1999) within the framework of the International Decade for Natural Disaster Reduction in the 1990s. Its objective was to develop earthquake damage scenarios and action plans in nine case-study cities selected worldwide. In the US one of the firts efforts in determining seismic risk scenarios was developed by the Applied Technology council in the California region. The ATC-13 (Applied Technology Council 1985) report defined a damage factor based on the estimates from 70 senior experts on the seismic performance of 78 existing facilities in California. The damage factor was defined as the ratio of dollar loss to replacement in percentage. Each expert was asked to provide an estimation of the damage factor for each facility at different Modified Mercalli intensities. The results of all experts were weighted and averaged to determine the probable damage factor expected to a certain facility given a Modified Mercalli Intensity. As an evolution of the ATC-13, the ATC-21 (Applied Technology Council 1996; McCormack and Rad 1997) also presents a scoring system based on visual observations with a rapid screen procedure. In this methodology first a basic structural hazard score is assigned depending on the structural type and the hazard on site. Next this basic score is modified to account for specific features that will induce a poor seismic performance. Finally, a structural score would be assigned by adding the Performance modifiers to the basic structural score. In both ATC documents, the index-based procedures present an objectivity issue since results are founded on the subjective analysis of an engineer. The latest methodologies overcame this issue by using approximate models and evaluating the performance of typical structures with sound

engineering methodology already implemented in current standards. Hazard United States or HAZUS (Federal emergency management agency 2018; Kircher, Whitman and Holmes 2006) is a software that implements a methodology for the estimation potential losses from earthquake events. The physical damage in structures is defined by estimating the probability of reaching None, Slight, Moderate, Extensive, and Complete damage to general building stock. The building stock is divided in 36 categories, depending on the structural material (steel, concrete, masonry, or timber) and height (low, mid or high-rise) and structural type (frames, walls, etc). Each of the 36 typologies has a probable capacity curve associated, which will be used for the prediction of the inelastic response of the structure with nonlinear static procedures (American Society of Civil Engineers 2000; Applied Technology Council 1996; Chopra and Goel 1999; Fajfar and Gašperšič 1996; Federal Emergency Agency 2005; Freeman 1998), resulting in the spectral displacement expected for a certain hazard level. This engineering demand parameter will be used for the estimation of the damage associated by means of a fragility curve defined for each of the 36 typologies. Compared to previous depicted vulnerability methods built on subjective inspections of buildings, HAZUS hinges on sound engineering procedures like the Capacity Spectrum Method (Freeman 1998) which proved effective in the estimation of the inelastic response of the structures. Analogously to the HAZUS Program in US, the European project Risk-UE (Moroux and Le Brun 2006) aimed to develop a modular methodology for constructing earthquake-risk scenarios, taking into consideration the features of European cities. The project focused on the performance of both conventional and historical buildings and the economic and social impact in the event of an earthquake. To estimate the vulnerability of conventional building Risk-UE proposes a hybrid method (Kapos el al. 2006) with two levels of approach: 1) based on damage data from field

observations after an earthquake or from experiments. And 2) based on feasible numerical models of representative structures.

As we have seen, the most advanced methodologies up to date rely on the performance of typical structures that represent the behaviour of all the structures alike, assuming that they provide a reasonable benchmark for the response of each individual building in the area under study: particularities of individual buildings are always masked within each typology group. These methodologies are typically recommended for large scale evaluations and a level of uncertainty should be acknowledged when applying it. Despite these disadvantages, earthquake and loss scenarios are powerful tools to support efficient seismic mitigation policies. At the regional level, adequate planning surely contributes to improve resilience with preventive and post-earthquake measures.

Because inspection of many buildings individually is time consuming and requires a dedicated workforce, researchers have made considerable contributions based on tools such as geographic information systems (GIS), computer models, data mining, or deep learning. Some examples are: Rajarathnam and Santhakumar (2015) developed a methodology to analyse and predict the seismic vulnerability of buildings with five storeys and above in Chennai from aerial photos. Gentile and Gallaso (2020) introduce a Gaussian process for seismic assessment of building portfolios. Flores, Escudero and Zamora-Camacho (2021) implement in Puerto Vallarta (MX) a GIS-based multicriteria evaluation model for seismic assessment. Kim et. al (2020) optimize a geoprocessing framework to characterize seismic site effects in Daejeon City (South Korea). Gonzalez et al. (2020) use deep learning models in street-view images to classify building typologies. Riedel et al. (2015) apply association rule learning and support vector machine methods for the seismic vulnerability assessment of urban environments. Borzi et al. (2011) show that satellite remotely sensed images are a powerful tool in the

vulnerability analysis of large industrial areas. Today, the use of GIS features is essential in vulnerability assessments worldwide: Azores (Ferreira, Maio and Vicente 2017), Bam (Hashemi and Alesheikh 2011), Barcelona (Lantada et al. 2010), Bogota (Riaño et al. 2021), Granada (Feriche 2013), Lorca (Torres et al. 2019), Manila (Quinay, Soliman and Fader 2020), Tabriz (Karimzadeh et al. 2014) or Weinan (Liu et al. 2014).

European geospatial infrastructure systems have rapidly evolved in the last 10 years. Today everyone can access massive geospatial data. In the case of buildings, the digital cadastral databases (Directive INSPIRE 2007; Van Loenen and Grothe 2014) combine location, geometric attributes, and temporal information. This data alone can be used to derive the main characteristics of the lateral carrying system of the buildings, and to assemble simple structural models and forecast seismic losses. This paper proposes an automated framework to estimate seismic vulnerability of large datasets of buildings from massive cadastral data.

Unlike traditional seismic vulnerability methodologies, which rely on collecting building data through time consuming surveys and visual screening, the first hypothesis in this paper is that available digital geodata in European cadastral databases provides sufficient information on the lateral carrying system of the buildings to assemble structural models. It is obvious that a detailed structural model cannot be derived from such limited information, but data allows for the estimation or deduction of several key values which define the mechanical and dynamic properties of buildings. Cities worldwide have seen great expansions in the second half of the 20th century, and these expansions have gone hand in hand with the enactment of seismic and building codes. The result is that existing residential and housing units are built upon well-known structural typologies and materials.

The proposed framework forecasts and quantifies seismic damage and earthquake losses, yet results are subjected to limitations. First, the insurmountable challenge of any seismic assessment methodology: the unpredictability of seismic action. Second, simplified models can hardly capture important phenomena such as soft story, short columns, brittle failures, atypical structures, among others. Consequently, there are uncertainties in the evaluation process that must be preserved, and outputs from individual buildings can be regarded as less plausible than overall or global results.

The seismic performance of the study region has been addressed scarcely in the literature. Based on seismic micro zonation data and the Vulnerability Index Method, Feriche (2013) derived vulnerability maps and seismic scenarios for the city of Granada. The discussion of the case study compares the results of that study with the proposed framework.

Research methodology

In brief, this framework essentially associates to each building item of the cadastral data (Directive INSPIRE 2007; Van Loenen and Grothe 2014), the probability of incurring in some level of seismic damage (e.g., negligible, slight, moderate, extensive) and the associated repair costs. The framework is implemented with the python toolbox pandas (McKinney 2015) and QuantumGIS (2021) and broken down into the steps in Fig. 1: i) Characterization of the seismic hazard by means of the seismic response spectrum at site, ii) Collection and processing of the cadastral data to obtain defining parameters of the building; iii) Estimation of a probable/representative capacity curve based on the cadastral data and the seismic design provisions existing at the time of construction, iv) assessment of the maximum lateral displacement by applying the non-linear static procedure in Eurocode 8 Annex B (European Committee Normalization 2004) and v) Prediction of the damage levels and economic losses. Each of the steps are further

explained below.

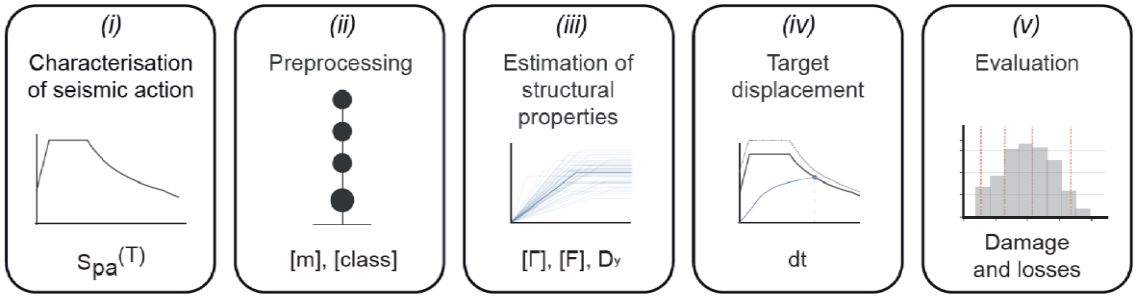

Fig. 1: Steps in methodology.

The presented framework is grounded on well-known seismic performance procedures, but it relies on GIS-based simplistic building models. To overcome this limitation, the framework is designed to acknowledge the inherent uncertainties in the problem. The uncertainties in significant structural parameters such as the fundamental period and the lateral capacity are accounted for by introducing a statistical variability with the Monte Carlo method. Because uncertainty is preserved in all the steps, the result is a probabilistic quantification of the buildings lateral displacement, damage states and repair costs. The outputs can be readily imported as attributes into geographic information systems, allowing for advanced analysis and visualization of the seismic damage scenarios. Because the framework translates seismic demand parameters into decision variables such as damage and losses, it can be applied to decision-making, policies, and strategies of seismic retrofit.

Characterization of seismic action

Seismic action is characterized as conventional elastic response spectra. Unless more detailed data is available, it is suggested to follow the harmonised provisions of Eurocode 8 (European Committee Normalization 2004) and its national annexes. The input parameters to define seismic action are: the shape of the response spectrum, the reference peak ground acceleration on stiff rock, the importance factor equalling unity, a 5%

viscous damping ratio of the structure, and the ground type at the building location in correspondence with available geotechnical and soil data. The spectrum is conventionally defined a piece-wise function of the fundamental period, divided into period ranges (e.g.: constant acceleration range, constant displacement range).

Fetching and pre-processing of the geospatial database

The initial step is to download massive cadastral geodata for the study area in order to extract the features of each building. The source of geospatial data must follow the INSPIRE directive cadastral specifications. The directive (Directive INSPIRE 2007; European Commission Joint Research Centre 2014) addresses 34 spatial data themes for environmental applications, including harmonized data specifications for buildings and cadastral parcels. The geospatial database consists of i) vector data with external building boundaries and internal building boundaries due to different number of floors as shown in Fig. 2, and ii) attribute data such as the number of floors, building parts, gross area per floor, building use, and year of construction as summarized in Table 1.

Table 1. Sample of the attributes in the geospatial database for the example building.

Cadastral Reference	Use	Year	Gross floor area (m^2)
7433601VG4173C	Residential	1970	3053

	Vol_1	Vol_2	Vol_3	Vol_4	Vol_5	Vol_6	Vol_7	Vol_8
Number of floors	9	2	2	10	8	8	8	8
Area (m^2)	272	4	14	24	12	8	17	4

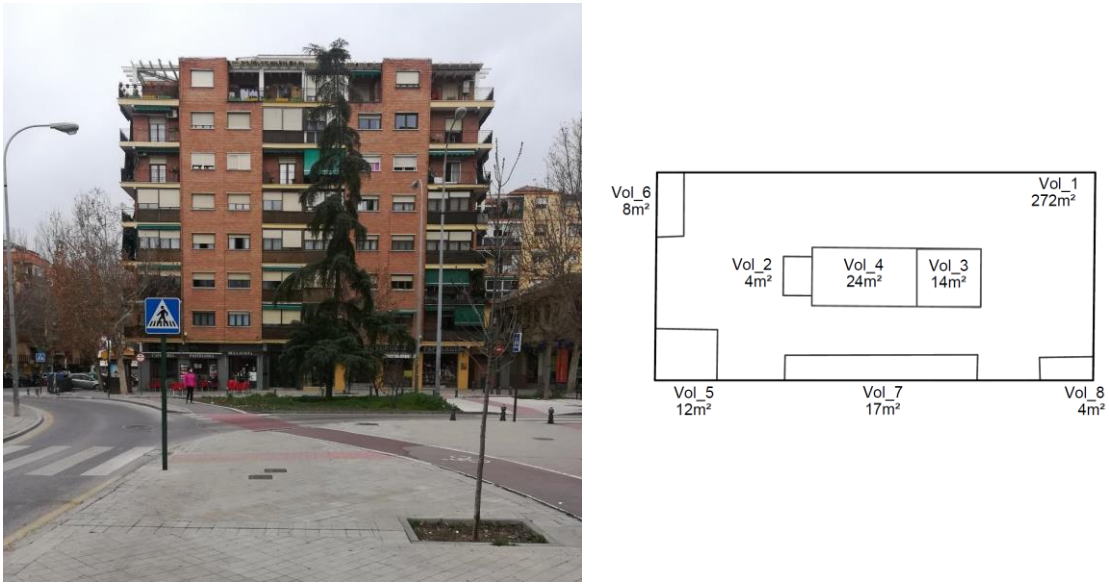

(a) (b)

Fig. 2: Sample of the vector data in the geospatial database.
Fig. 2(a): Example building.
Fig. 2(b): Vector data.

It is hard to envisage that a thorough structural model can be derived from such limited information, but the cadastral data allows for the estimation or deduction of several key values to approximately define the mechanical and dynamic properties of buildings:

- The construction year gives an insight of the ruling standard under which the structure was designed. Hence the resistance requirements of the buildings at that time, which can be condensed with the base shear coefficient or seismic coefficient for brief.
    - Structural typology. Standardization and the evolution of the codes of practice over the years have narrowed down the number of structural typologies in conventional buildings, resulting in a strong homogenization of the building technologies. Furthermore, structural design has been heavily regulated by building codes in the 20th century. Therefore, although the structural typology may not be given by cadastral data, it is straightforward to assign a structural type based on the building geometry and the construction practice around the year of construction. This can be achieved by a classification algorithm considering the

design provisions of the local codes, the year when they were adopted, and engineering knowledge on the local building technology. A straight-forward classification algorithm is illustrated in Fig. 3, where each dot represents a building. In this example, buildings are categorized depending on the year of construction and the maximum number of floors. Sophisticated classification algorithms capable of detecting nonductile typologies are readily available in the literature (González et al. 2020).

- Mass vector. The number of stories together with the gross area per floor and the typical weights of materials provide a close estimation of the mass distribution along the building height. Hence enabling for an estimation of the seismic mass vector [m], closely related to the vibration modes and the forces on the structures.
- Fundamental period: may be approximated from well-known empirical expressions accounting for the building height and structural typology.

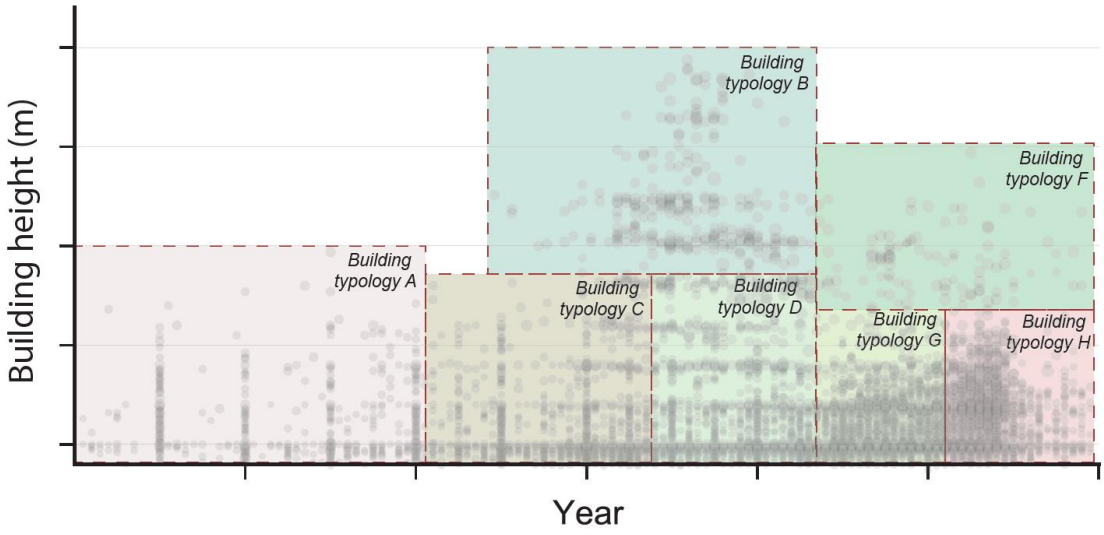

Fig 3: Example of classification algorithm.

As a result of pre-processing the attribute data of each building in the region under study, it is possible to assemble a lumped seismic mass vector [m] proportional to the gross floor area and assign a structural typology which will be further needed to estimate the lateral

capacity of the structural system. The results of the framework rely on prior engineering judgement on the building typologies and on the seismic regulations in the study area. It is advisable to preselect a reasonable sample set of representative buildings and to compare the parameters with alternative analytical models.

Estimation of structural capacity curves

Capacity curves are one common way to characterize structural lateral capacity because they relate base shear force F_b and roof drift D under monotonically increasing lateral forces. Regarding capacity, there are 3 characteristic points in the typical pushover curve shown in Fig. 4: design capacity F_d, yield capacity F_y, and ultimate capacity F. Capacity curves are usually idealised as elastic-perfectly plastic models regardless of post-elastic stiffness, as shown with red dashed lines. As a result, only two structural parameters are needed to estimate a simplified capacity curve: the ultimate capacity F, and the yield lateral displacement D_y. The lateral design capacity F_d can be estimated with Eq. (1) as the product of the design base shear coefficient c and the effective mass of the building in the first mode of vibration, $M_{eff,1}$. The design base shear coefficient can be deduced by mimicking the design process in the corresponding building code. The effective mass in Eq. (2-5) is derived from the transformation factor Γ_1, the modal mass M_1, and the modal participation factor L_1. The shape of the first mode of vibration φ_1 can be taken as $\sin(x)$ for $x \in (0, \pi/4)$.

The ultimate capacity of the lateral bearing system F in Eq. (6) is derived multiplying the design capacity F_d by the empirical factors γ_1 and γ_2 [6]. Γ_1 is an overstrength factor that relates the design to the yielding strength and γ_2 an overstrength factor relating the yielding to the ultimate strength. The last parameter to define the idealized bilinear capacity curve is the yielding displacement D_y of the structure, which depends on the structural type. In conventional buildings, the typical values proposed in

HAZUS and FEMA 356 (American Society of Civil Engineers ASCE 2000; Federal emergency management agency 2018; Kircher, Whitman and Holmes 2006) for reinforced concrete and masonry buildings can be adopted, in the range 0.5% and 0.25% respectively of the total height of the building.

$$F_d = c \cdot M_{eff,1} \quad \text{Eq. (1)}$$

$$M_{eff,1} = \Gamma_1^2 \cdot M_1 \quad \text{Eq. (2)}$$

$$\Gamma_1 = L_1 / M_1 \quad \text{Eq. (3)}$$

$$M_1 = [\varphi_1]\,[M]\,[\varphi_1] \quad \text{Eq. (4)}$$

$$L_1 = [\varphi_1]\,[M]\,[1] \quad \text{Eq. (5)}$$

$$F = \gamma_1 \cdot \gamma_2 \cdot Fd \quad \text{Eq. (6)}$$

Finally, in order to account for the uncertainty in the definition of the capacity curve, a probabilistic approach is adopted. For each individual building 50 capacity curves were randomly obtained using a Monte Carlo simulation by varying the values of F and D_y within certain bonds. Depending on the year of construction a variability in F and D_y of ± 30% and ± 20% was considered for pre-code and code designed buildings respectively, as recommended in HAZUS (Federal emergency management agency 2018, Kircher, Whitman and Holmes 2006). Fig. 4(b) shows an example of one pre-code individual including all the capacity curves obtained in the process, the mean capacity curve and a shadowed area covering the mean ± 1 standard deviation. Each of these curves is used to the probable performance of the building.

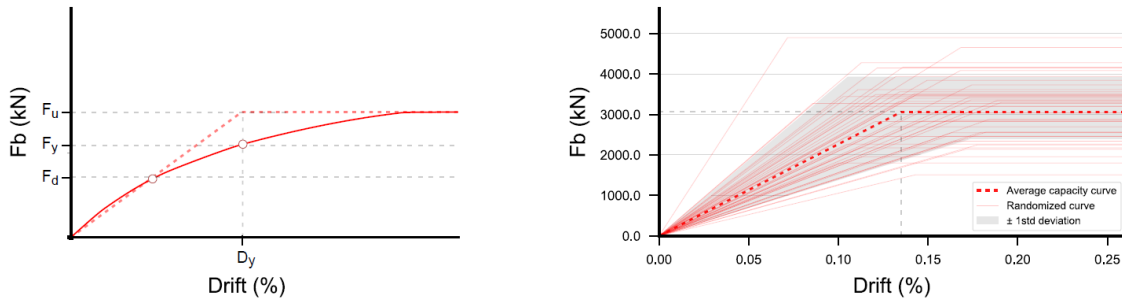

(a) (b)

Fig. 4: Capacity curves:(a), Idealisation of a capacity curve, (b) Probabilistic capacity curve.

Calculation of the target displacements

Experimental and numerical research (Calvi, Priestley and Kowalsky 2007; Fardis 2009; SEAOC Seismology Committee 2006) on the seismic performance of structural components has proven that damage is directly related to the maximum lateral displacement or drift demand during an earthquake. Therefore, the accurate assessment of the displacement demand in structures has been a main goal in displacement-based design methodologies. Several researchers have proposed simplified nonlinear static procedures based on push over analysis which provide reasonable estimations of the maximum displacements expected during an earthquake (American Society of Civil Engineers ASCE 2000; Applied Technology Council 1996; Chopra and Goel 1999; Federal Emergency Agency 2005; Freeman 1998). The N2 method proposed by Fajfar (1996) and adopted in Eurocode 8 (2004) is implemented in this study. First step in N2 is to transform the capacity curve of the multiple degree of freedom system obtained above into the capacity curve of an equivalent system with a single degree of freedom by means of Eq. (7,8)

$$F^* = F/\Gamma \qquad \text{Eq. (7)}$$

$$d^* = d/\Gamma \qquad \text{Eq. (8)}$$

Then, the fundamental period T^* of the equivalent single degree of freedom system is readily obtained.

$$T^* = 2\pi\sqrt{\frac{L_1\, d_y^*}{F_y^*}} \qquad \text{Eq. (9)}$$

Next, using the spectral acceleration $S_e(T^*)$ given by the site elastic response spectrum, the elastic displacement, d_{et}^*, of the equivalent single degree of freedom system would be:

$$d_{et}^* = S_e(T^*)\left(\frac{T^*}{2\pi}\right)^2 \qquad \text{Eq. (10)}$$

Finally, the expected inelastic displacement, d_t^* , is determined by means of Eq. (11-12), depending on whether the equivalent single degree of freedom fundamental period lies in the range of short ($T^* < T_c$) or medium to long periods ($T^* \geq T_c$). T_c is the transition period between short and medium to long periods, and q_u in Eq. (13) is the ratio of the force demand if the structure behaved elastically to the yielding force. Finally, the actual displacement *d* of the multiple degree of freedom system is determined with Eq. (14) by undoing the transformation in Eq. (8).

$$d_t^* = \frac{d_{et}^*}{q_u}\left(1 + (q_u - 1)\frac{T_c}{T^*}\right) \geq d_{et}^* \qquad \forall\, T^* < T_c \qquad \text{Eq. (11)}$$

$$d_t^* = d_{et}^* \qquad \forall\, T^* \geq T_c \qquad \text{Eq. (12)}$$

$$q_u = \frac{S_e(T^*)\, L_1}{F_y^*} \qquad \text{Eq. (13)}$$

$$d = \Gamma\, d_t \qquad \text{Eq. (14)}$$

Assessment of seismic performance

The last step in the framework is to categorize building damage as a function of the target displacement predicted above. Five damage states (DS) defined in Hazard United States (HAZUS) are adopted in this study i.e.: no damage (DS_0), light (DS_1), moderate or life safely (DS_2), extensive or immediate occupancy (DS_3) and complete (DS_4). The threshold between each of these damage states is associated to a value of the lateral displacement in terms of drift depending on the characteristics of the seismic resistant systems. Hence, the probable damage that an individual would incur will be the most likely damage obtained from comparing the displacement predictions in previous section to pre-set limits. Figure 5 shows a histogram of drift ratios obtained for the set of 50 probable capacity curves representing the lateral behaviour of an example building, together with the drift limits for the structural typology of the building. From this histogram it is

possible to derive the probability of incurring in a certain damage state. In this example, the strongest likelihood (representative damage) is that the earthquake action results in extensive damage state (DS_3).

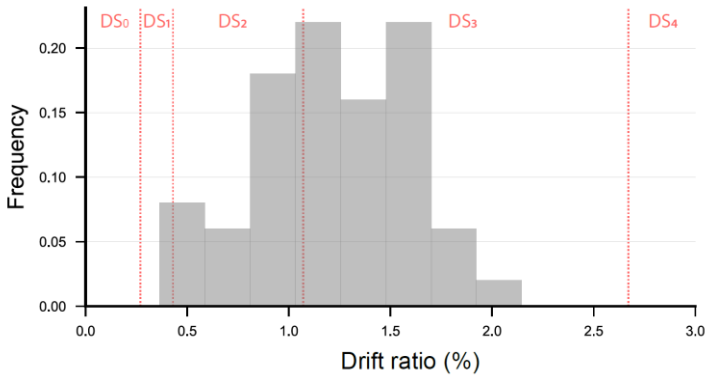

Fig. 5: Probability distribution of drift ratios in an example building.

The framework can forecast several metrics, such as human losses, environmental impacts, or repair costs. This can be done by using models that relate seismic damage states (DS) with occupation, life cycle assessment, unitary repair costs or fragility curves. For the sake of simplicity, this paper shows an implementation able to estimate repair/retrofitting costs based on a statistical relationship between damage states and repair costs proposed by Cimellaro et al. (2010). More sophisticated models to forecasts other metrics are readily available in the literature (Applied Technology Council 2018).

According to Cimellaro et al. (2010), seismic repair costs can be roughly calculated as a percentage of the initial building investment. Recovering from DS_1, DS_2, DS_3 and DS_4 can be taken as cost factors: 15%, 38%, 76%, and 106% respectively of the building construction cost. The construction building cost can be approximated as the product of the gross floor surface and the construction cost by surface unit. Finally, the seismic repair costs for a building can be estimated from the distribution of the 50 probable damage states above. By multiplying the building construction cost by the cost factor corresponding to each damage state, we obtain a distribution of 50 probable repair

cost values. Following the same reasoning, the framework may quantify other variables such as downtime, environmental impacts, or damage to household belongings.

Case Study: the metropolitan area of Granada

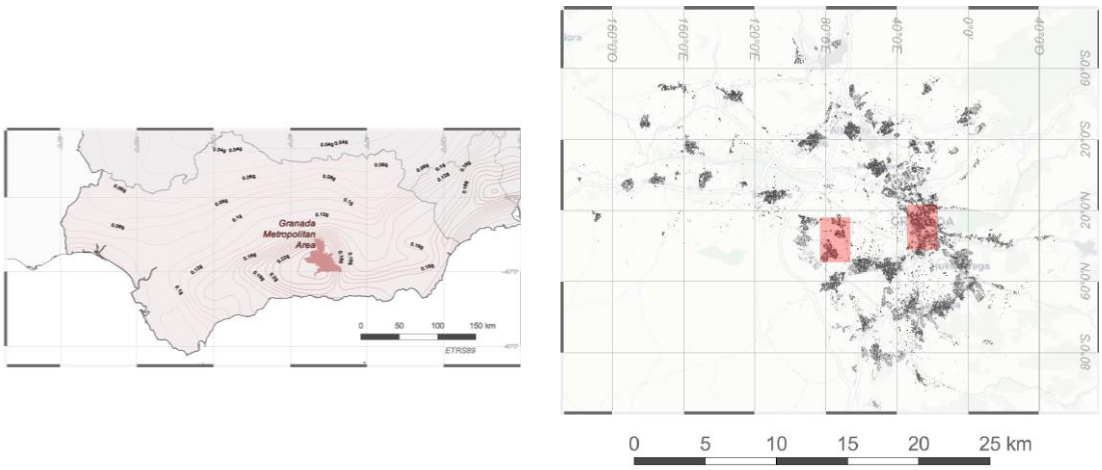

(a) (b)

Fig. 6: Maps of Granada Metropolitan Area: (a) Andalucía 475-year return period hazard map (EC-National Annex), (b) Urban areas

The metropolitan area of Granada (Andalucía, Spain) in Fig. 6 comprises 32 municipalities with an estimated population of 530,808 people. According to cadastral information, there are 287,503 housing units, summing up to a floor surface of roughly 47 million square meters. Granada is a historic city dating from the 7th century BC and has a significant amount of heritage monuments and places of great historical interest. The metropolitan area has seen a great expansion in the second half of the 20th century, with a 15-fold increase of the gross floor housing area in the period 1950-2010, from 3 to 45 million square meter in the period at a yearly rate of 700,000 square meter. Figure 7 shows the evolution of the gross housing floor stock in the metropolitan area, and the enforcement of seismic codes with red dashed lines.

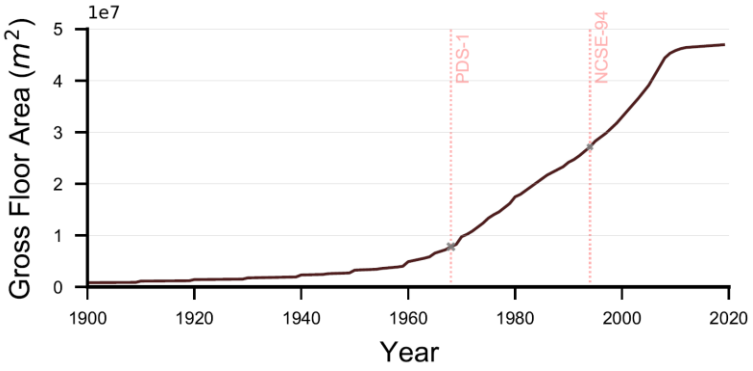

Fig. 7: Evolution of the housing gross floor area in the Metropolitan area of Granada.

The housing stock is exposed to earthquake hazard sourcing from well-known seismic faults (Montilla, de Galdeano and Casado 2003) responsible of destructive ground motions in recent history. The current seismic hazard map of Spain for a probability of exceedance of 10% in 50 years prescribes the highest peak ground acceleration in the country for the metropolitan area of Granada. In Spain we can consider that there are three milestones on the seismic design of buildings, coincidental to the publication dates of the seismic standards. First, all buildings built before 1963 when proper design regulations did not exist, and it is assumed that designed followed mere heuristic approaches. The first building code accounting for seismic action MV-101 (Ministerio de Vivienda 1962) comes into force in 1963, prescribing a design seismic coefficient of 10% of the building seismic weight. Shortly after, in 1968 the first seismic code PGS-1 (Presidencia del Gobierno 1968) increases the seismic coefficient, introduces spectral modal analysis, and describes masonry structures as non-compliant to seismic design. In 1974, this code is superseded by a minor revision PDS-74 (Ministerio de Planificación del Desarrollo 1974). Modern seismic codes are put in place in 1994 (Ministerio de Obras Públicas, Transportes y Medio Ambiente 1994) and revised in 2002 (Ministerio de Fomento 2002), increasing again the seismic coefficient and introducing capacity design and seismic response reduction factors (behaviour factor) with specific detailing

requirements for ductility. In comparison to newer standards as the Eurocode or ASCE 7, NCSE is rather limited today as it lacks provisions on plenty of lateral resisting systems, seismic isolation, capacity design rules, etc. After Lorca earthquake, the 475-year return period seismicity map of Spain was revised in 2015 but it is not yet enforced in the current code.

Figure 8 draws a comparison of design spectra in the different codes, contemplating different values of the seismic behaviour factor (namely q in Eurocode, factor R in American codes). Code MV-101 seriously underestimates seismic action, especially in the short period range. The design spectra in moderate-codes (PGS-1 and PDS-74) either underestimates seismic action or overestimates structural ductility, as it is comparable to the current spectrum in NCSE02 with a behaviour factor $q \sim 3.5$.

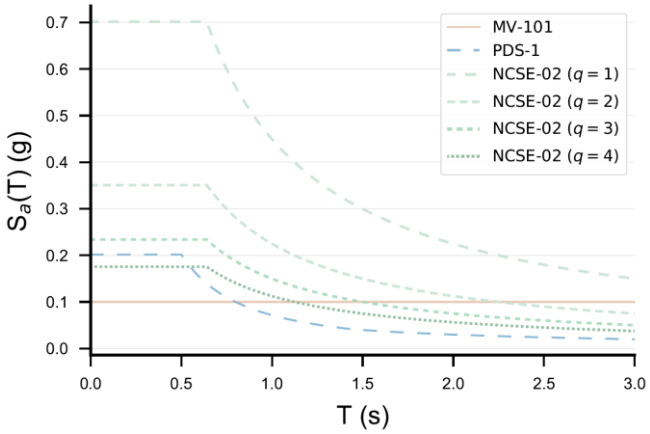

Fig. 8: Design response spectra in Spanish building codes MV101, PDS1, NCSE-02 with different values of the behaviour factor.

Due to restrictions in the seismic codes, most of the existing housing constructions are built on reinforced concrete frame structures. Standing on the expected seismic performance, the building stock of the metropolitan area can be categorized based on the year of construction, the structural typology, and the number of floors. The resulting categories are pre-code (PCODE) designed buildings before 1968, moderate code (MCODE) buildings between 1969 and 1994, and high code buildings (HCODE) since

1995. According to the structural typology, the predominant categories are unreinforced masonry (MA) and reinforced concrete frames (RC). Finally, the number of floors yields three categories: low, medium, and high structures (L, M, H). Figure 9(b) shows a disaggregation of the housing stock into 11 typological categories, being the most frequent HCODE.RC.L (23.9% of the gross floor area), MCODE.RC.L (16.5%), HCODE.RC.M (15.8%), MCODE.RC.M (13.0 %), MCODE.RC.H (10.6 %), PCODE.MA.L (9.2 %). The rest of the categories are below 5%. Figure 9(a) shows the distribution of story height in recent history and the distribution of categories and Fig. 10 shows two extracts of the map of building categories in the metropolitan area of Granada.

(a)

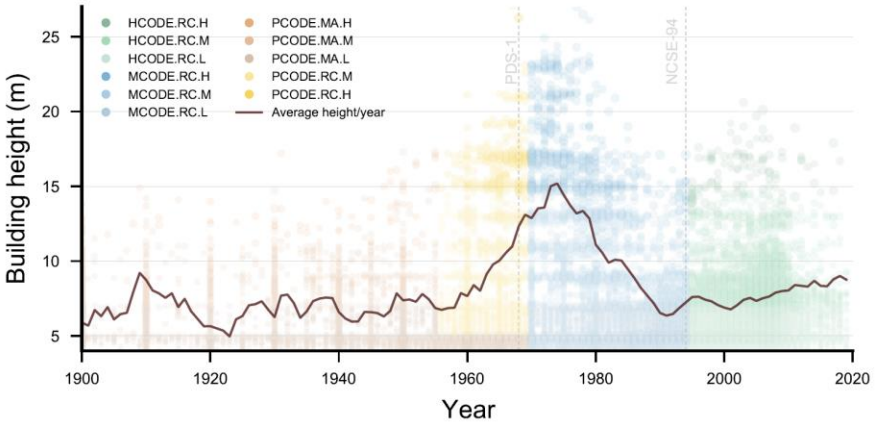

(b)

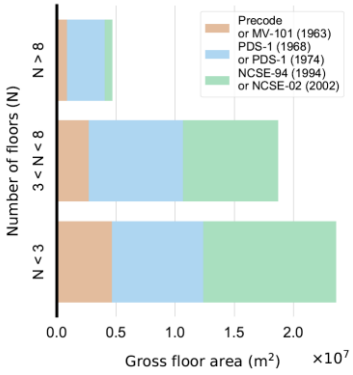

Fig. 9: Distribution of story height and: (a) number of floors, (b) seismic code.

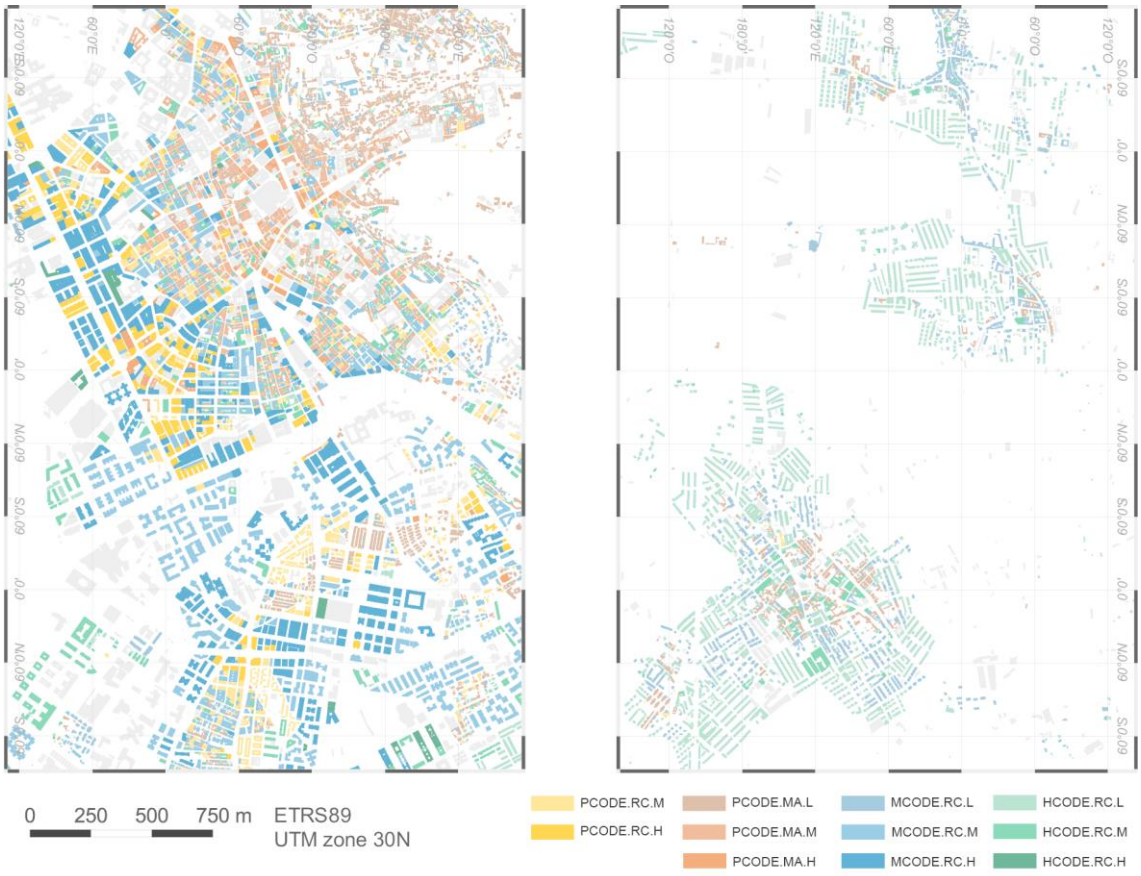

Fig. 10: Sample map of building categories in the metropolitan area of Granada.

Following the framework, the lateral capacity of each building structure is idealized as a set of 50 bilinear elastic-perfectly plastic curves with a predetermined variability using a random number generator. The median lateral strength is calculated by mimicking the design procedures in the corresponding seismic codes and applies overstrength and variability factors. A summary of these factors is shown in Table 2. The median yield displacement of these lateral systems is estimated from previous knowledge of the structural typologies as a percentage of the building height.

Table 2. Parameters related to the building's categories.

Code	Description	Year	Floors	γ_1	γ_2	β	D_y
PCODE.MA.L	Masonry low-rise precode building	Before 1956	[1, 2]	1.5	3	0.3	0.25
PCODE.MA.M	Masonry medium-rise precode building	Before 1956	[3, 5]	1.25	3	0.3	0.25
PCODE.MA.H	Masonry high-rise precode building	Before 1956	[6, 9]	1.1	3	0.3	0.25
PCODE.RC.M	RC medium-rise precode building	[1956, 1968]	[3, 7]	1.25	2	0.3	0.5
PCODE.RC.H	RC high-rise precode building	[1956, 1968]	[8, 12]	1.1	2	0.3	0.5
MCODE.RC.L	RC low-rise moderate code building	[1969, 1994]	[1, 3]	1.5	1.3	0.25	0.5
MCODE.RC.M	RC medium-rise moderate code building	[1969, 1994]	[4, 7]	1.25	1.3	0.25	0.5
MCODE.RC.H	RC high-rise moderate code building	[1969, 1994]	[8, 13]	1.1	1.3	0.25	0.5
HCODE.RC.L	RC low-rise highcode building	[1994, 2019]	[1, 3]	1.25	1.3	0.25	0.5
HCODE.RC.M	RC medium-rise highcode building	[1994, 2019]	[4, 7]	1.25	1.3	0.25	0.5
HCODE.RC.H	RC high-rise highcode building	[1994, 2019]	[8, 12]	1.1	1.3	0.25	0.5

For assessment purposes, seismic action is characterised by elastic response spectra calculated for Granada Metropolitan Area according to EC8, the latest official hazard map, the provisions of the National Annex of Eurocode 8, and engineering knowledge on the ground types. Seismic action corresponds to the design earthquake, with a probability of exceedance of 10% in 50 years (return period of 475 years). The current seismic code prescribes a peak ground acceleration (PGA) at stiff rock of 0.23g, which is converted to PGA at rock level by a factor of 0.8 as suggested in the Proposal of National Annex. Finally, the site-specific spectra can be calculated considering the soil type at the building location. Regarding the ground types, the Granada basin is composed by alluvial fans, colluvial deposits and conglomerates. Latest research on lithological units in the Metropolitan region (Valverde-Palacios 2010; Chacon et al. 2012; Valverde-Palacios et al. 2014) has revealed that the velocity of shear waves V_S consistently lies in the range V_S =250~350 m/s. According to the National Annex of Eurocode 8, a ground type C can be adopted across the study region, resulting in the elastic seismic response spectra in Figure 11.

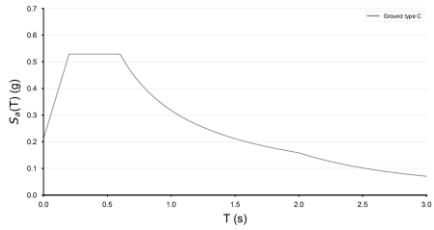

Fig. 11: Elastic seismic response spectra for ground type C (Vs=330 m/s).

So far, the procedure has associated to each housing building a seismic demand spectrum, and a set of 50 capacity curves to idealize its probable lateral behaviour. As a result, 50 possible performance points are calculated for each building, obtaining a statistical representation of the effects of the seismic demand on the building structure. For the sake of example, a summary of parameters related to the sample building in Figure 2 are shown in Appendix A. Figure 12 depicts a map of the median target displacements in two regions of the metropolitan area. These two regions are highlighted in red in Fig. 6(b).

Next, the set of 50 probable target displacements are converted into damage states by using the threshold values in Table 3. These values are taken from engineering judgement and the recommendations of HAZUS, allowing for larger threshold values in higher and more recent buildings. Four damage states are considered in the case study, namely: DS_1 Low, DS_2 Moderate, DS_3 Extensive, and DS_4 Complete. As a result, the procedure can estimate the representative or most frequent damage state, and the probability of exceeding the different damage states in each housing building.

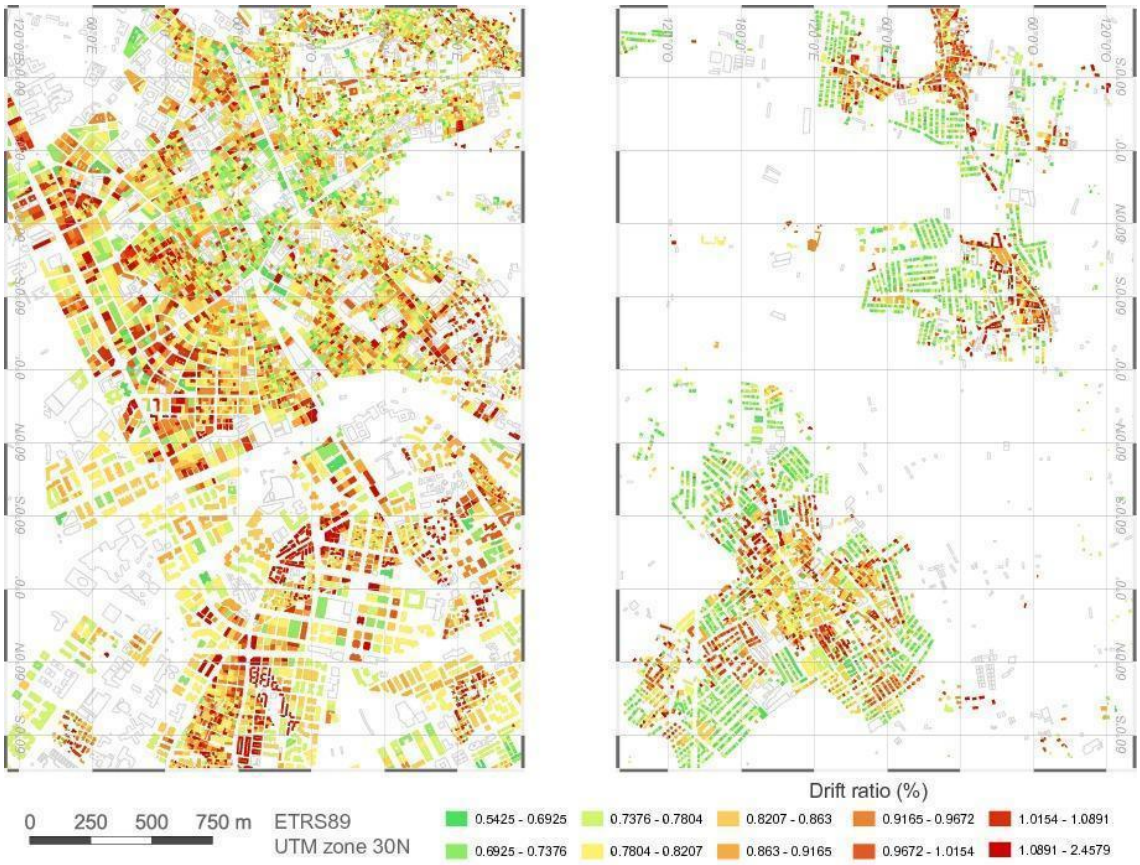

Fig. 12: Sample map of median target displacements as a percentage of the building height.

Table 3. Lateral displacement thresholds as percentage of the building height and corresponding damage states

Class	DS_1	DS_2	DS_3	DS_4
PCODE.MA.L	0.0032	0.0051	0.0128	0.0350
PCODE.MA.M	0.0021	0.0034	0.0086	0.0233
PCODE.MA.H	0.0016	0.0026	0.0064	0.0175
PCODE.RC.M	0.0027	0.0043	0.0107	0.0267
PCODE.RC.H	0.0020	0.0032	0.0080	0.0200
MCODE.RC.L	0.0050	0.0087	0.0233	0.0600
MCODE.RC.M	0.0033	0.0058	0.0156	0.0400
MCODE.RC.H	0.0025	0.0043	0.0117	0.0300
HCODE.RC.L	0.0050	0.0100	0.0300	0.0800
HCODE.RC.M	0.0033	0.0067	0.0200	0.0533
HCODE.RC.H	0.0025	0.005	0.0150	0.0400

The resulting estimation of damage states quantifies a clear tendency for better seismic performance in newer buildings (Fig. 13). Similar amounts of buildings show moderate damage in pre-code and moderate-code designs (92.7% vs 92.9%), but the number of buildings with extensive damage drastically decreases with moderate-code regulations. More importantly, buildings designed before 1994 show moderate damage in over 90% of the observed cases, dropping to 11% with the enforcement of NCSE-94. This tendency can be explained by the evolution of seismic codes, but it must be also related to the great deal of high-rise buildings in the moderate code period 1968-1994.

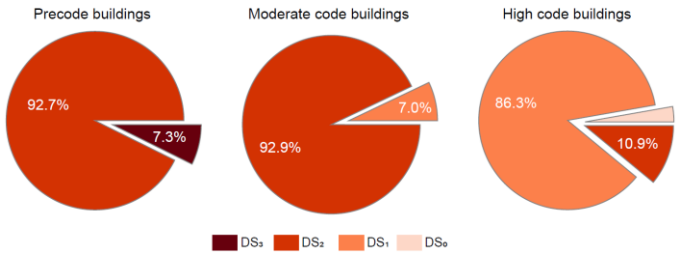

Fig. 13: Representative seismic damage under different seismic codes.

Figure 13 shows damage states in two sample maps of the metropolitan area. The results are disaggregated by building category in Fig. 14. Complete seismic damage is only observed in taller RC pre-code buildings, which represent the most vulnerable typology, followed by extensive damage in other pre-code buildings with masonry or RC structures. Regarding medium-code and high-code buildings, the most frequent observation is moderate damage, except for recent low-rise RC buildings, with minor damages. Regarding the building height, two and three-story buildings show the best overall performance. The expected levels of damage are particularly similar for all buildings taller than 4-5 floors.

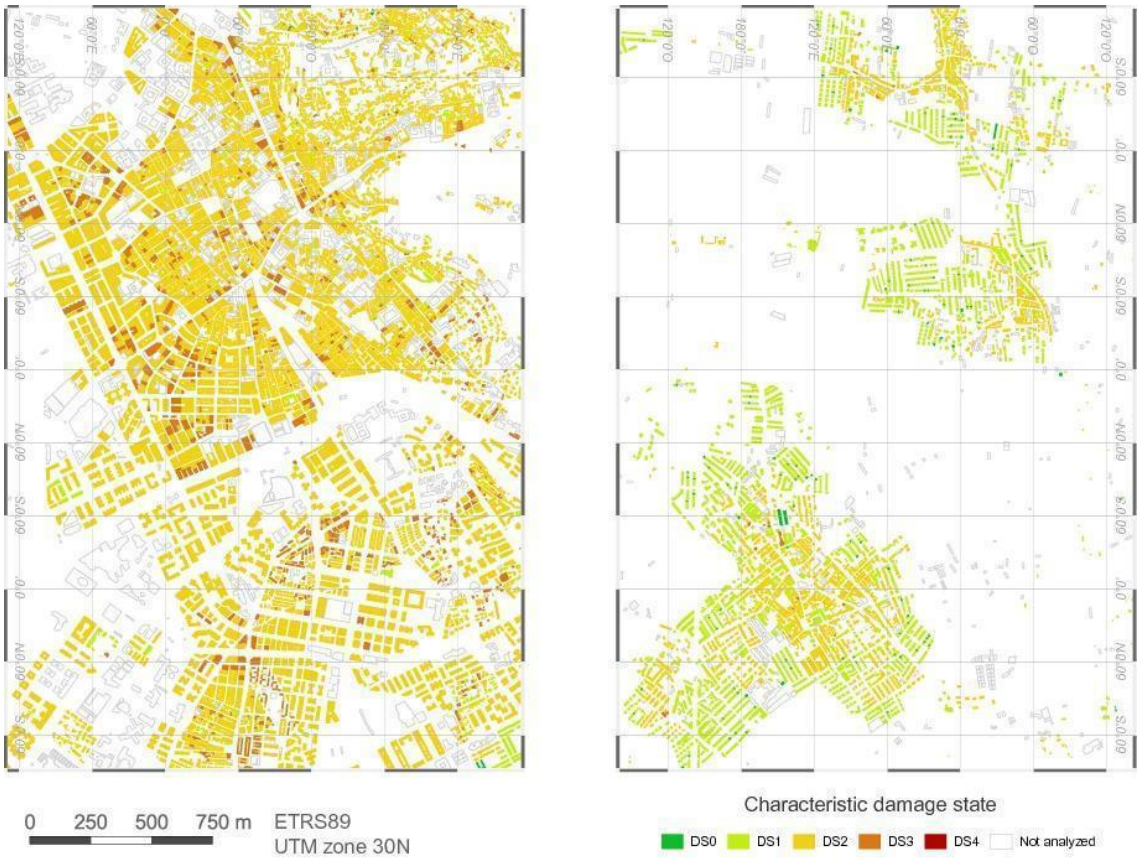

Fig. 14: Sample maps of representative seismic damage.

(a)

(b)

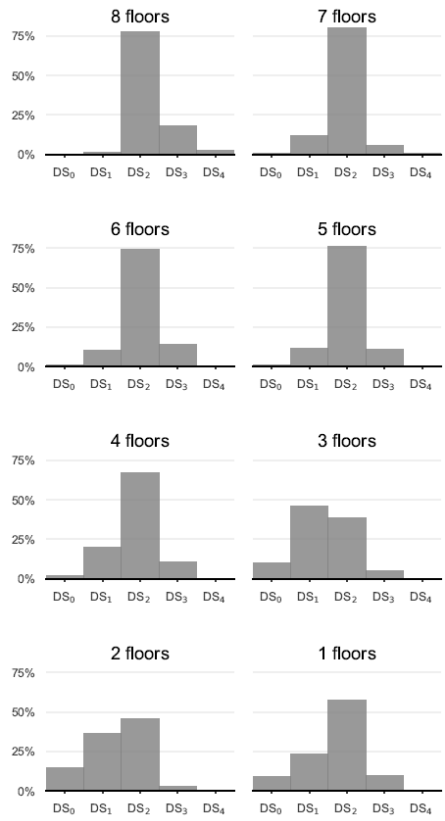

Fig. 15: Histograms of seismic damage (a) by building category, (b) by number of stories.

Building construction costs are calculated by assuming a flat cost of 600€ per square meter of building floor. The repair costs of home appliances and personal belongings is excluded. Recovering costs from DS_1, DS_2, DS_3 and DS_4 are taken as 15%, 38%, 76%, and 106%, respectively, of the building construction cost (Cimarello, Reinhorm and Bruneau 2010).

One of the most direct forecasts is that the median repair costs for the metropolitan area of Granada sum up to 9,376 M€. The 5%, 25%, 75%, 95% percentile values of the repair costs are respectively 4,149 M€; 6,881 M€; 10,457 M€;13,085 M€. On average, this is 32,612 € per household, and 17,664€ per capita. These figures seem reasonable in comparison to the outcomes of the 5.1 Mw near fault earthquake that struck Lorca (Murcia) in 2011: 568M€ in compensations only for 33,200 damaged properties

(17,108€/property) according to the official report by Cabal (2013), yet further reports in 2019 reckon that reconstruction costs are up to 1200M€.

Figure 16 shows a box and whiskers plot with 5, 25, 50, 75 and 95 percentile values of the percentage of economic losses by municipality in the metropolitan area. On average, median economic losses amount to 33% of the initial construction investment. The general trend in municipalities is that median losses are about 25-30%, except for Granada rising to 40% due to the amount of deprecated structural designs and vulnerable buildings.

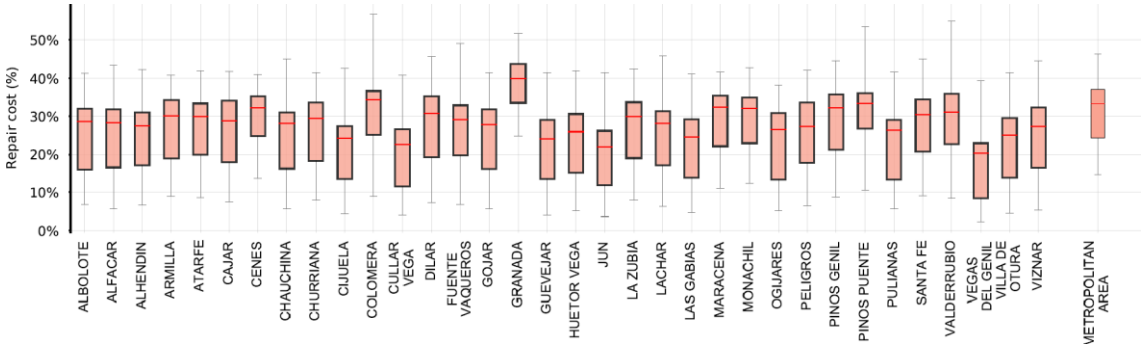

Fig. 16: Percentage of seismic losses by municipality.

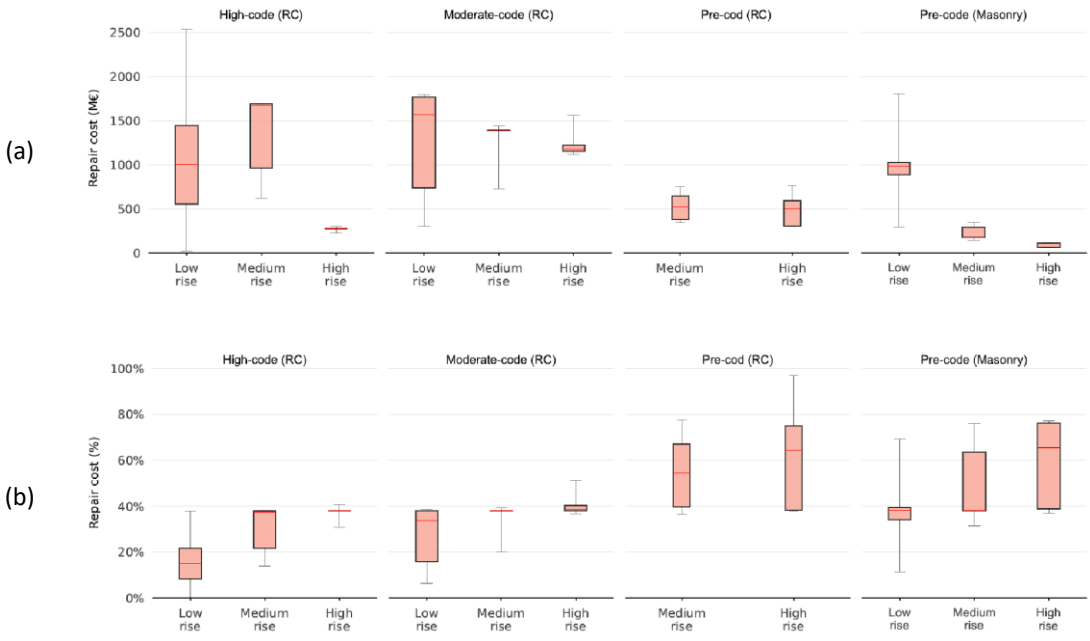

Fig. 17: Disaggregation of repair costs by building typology: (a) as % of the initial building cost, (b) as total costs.

Repair costs concentrate on vulnerable buildings and/or densely populated areas with a higher buildability, which are highlighted in red in the heat map in Figure 18. In the case of the municipality of Granada (left map) repair costs concentration occurs around pre-and-moderate code high-rise buildings in the Ronda district, summing up to 125M€ in a 125m diameter. Smaller municipalities such as Cullar Vega (right map, bottom) concentrate seismic losses mostly around pre-code masonry buildings in the historic city centres, yielding about 8 times less cost concentration.

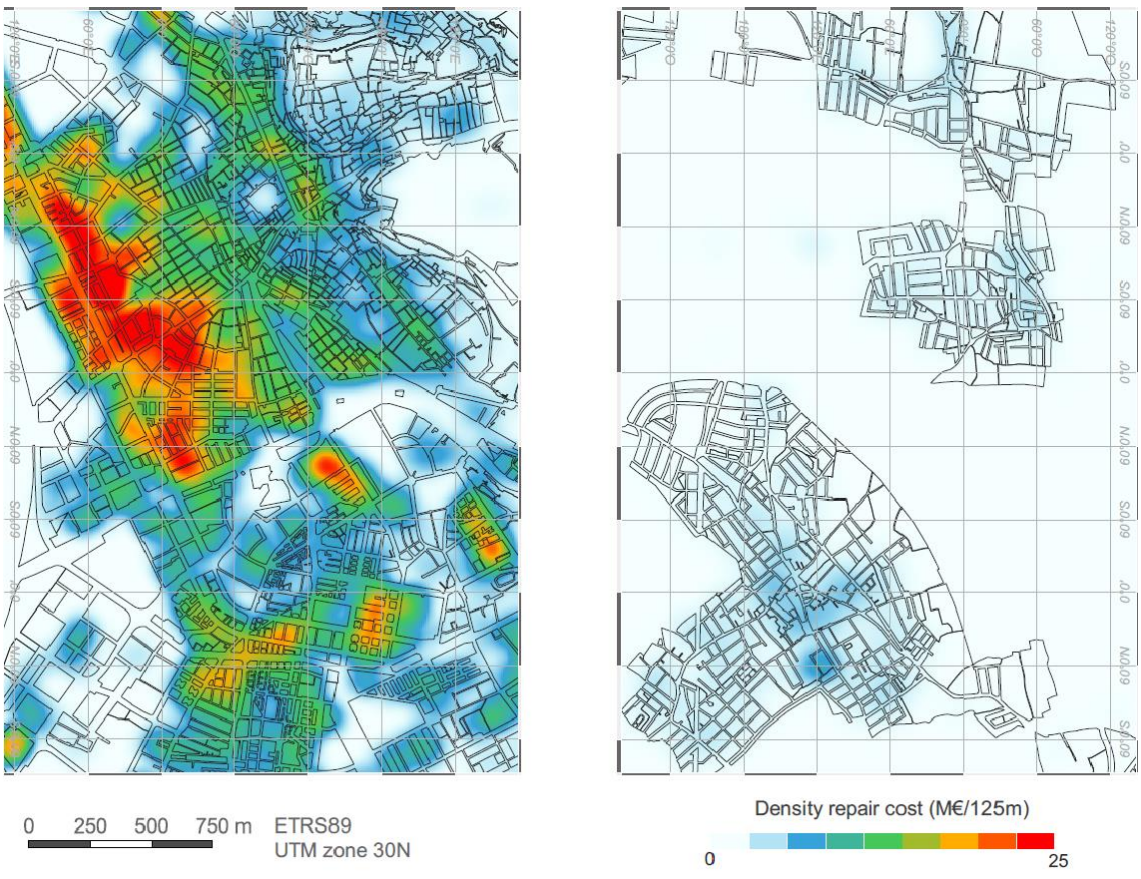

Fig. 18: Heatmap of seismic repair costs.

Because of the different assessment approaches, results obtained in the case study are hard to compare with available literature. Feriche (2013) estimated seismic scenarios

for the municipally of Granada based on the Vulnerability Index Method with 16~20 modifiers and semi-empirically calibrated vulnerability curves, resulting in the seismic damage map in Fig. 19 (b) and the disaggregation of damaged buildings in Fig. 20 (b) under the action of a 475-year return period strong motion. The results of the proposed framework (municipally of Granada only) are shown in Fig. 19 (a) and Fig. 20 (a). In comparison, both methodologies show widespread moderate damage in residential buildings, and most differences are due to the fact that Feriche contemplates a larger variety of building uses (cultural, religious, heritage, sport, industrial) that fall outside the scope of the proposed framework (residential only). Paying closer attention to urban areas, there are remarkable coincidences in neighbourhoods 1 and 2, highlighted with dotted black lines in Fig. 19. Specifically, in neighbourhood 2 the framework seems to capture more details on the urban fabric, and forecasts poorer seismic performances associated to masonry buildings from the 1950-60s (autarky housing).

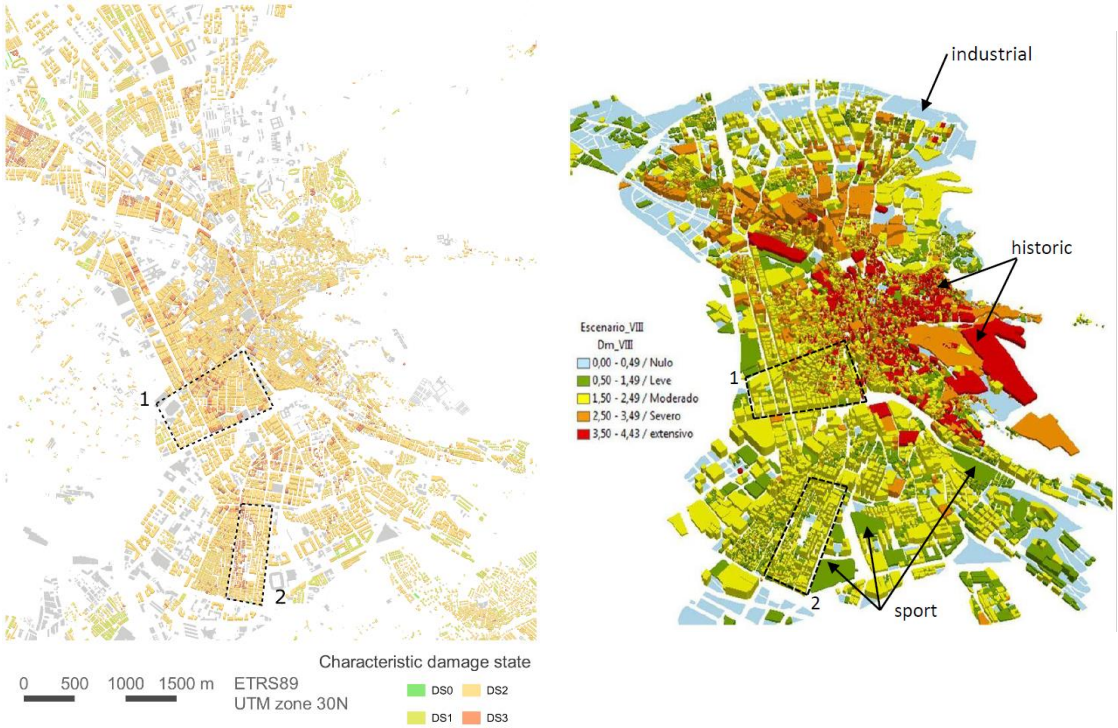

Fig. 19: Seismic damage maps (a) case study, (b) Feriche 2013

Regarding the disaggregation of damaged buildings in Fig. 20, there are some differences to discuss. First, the framework analyses only residential buildings, and is not taking into account the contribution of historic buildings (in extensive damage), industrial buildings (negligible damage), and other sport and public facilities (minor damage). Second, the framework forecasts a poorer seismic performance in 2-storey buildings which seems to follow the general trend of the results.

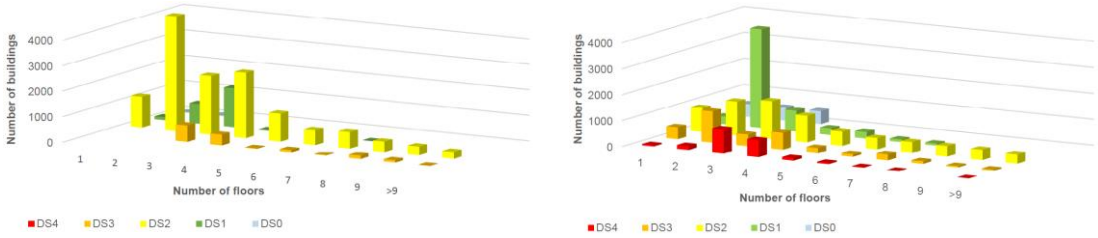

(a) (b)

Fig 20. Disaggregation of buildings by number of floors and damage states: (a) proposed framework, (b) Feriche 2013.

Conclusions

The proposed framework forecasts and quantifies seismic damage and earthquake losses from cadastral geospatial data and relies on fundamental theories of earthquake engineering. In comparison to other methodologies, the presented framework is i) computationally rapid (assessment of 287,503 housing units within minutes on a domestic computer), ii) based on sound displacement-based procedures, iii) takes into account irregularities in the building structure, iv) provides a probabilistic approach to seismic damage and losses, v) can be easily applied to other European regions, vi) can be expanded to account for environmental, occupational or social metrics, and vii) is developed on free software.

The application to the metropolitan area of Granada showcases the power of the framework in a medium-seismicity 972.62 km² region. After fetching the INSPIRE cadastral database of the region, the framework classifies the housing building stock into 12 structural typologies. Inside each typology, the main characteristics of the lateral resisting system are calculated by implementing the design procedures in the corresponding buildings codes enforced in 1962, 1968, 1974, 1994, and 2002. A Monte Carlo procedure is included to preserve the inherent uncertainties in the problem, resulting in a set of 50 probable capacity curves, 50 probable damage states, and 50 probable estimations of seismic losses per building.

The framework describes damage in increasing steps: low, moderate, extensive, and complete. The most observed damage state in pre-code and moderate-code buildings is moderate damage (93% of cases), although the number of buildings with extensive damage drastically decreases with moderate-code regulations. More importantly, buildings designed before 1994 show moderate damage in over 90% of the observed cases, dropping to 11% with the enforcement of NCSE-94. This tendency can be explained by the evolution of seismic codes, but it must be also related to the great deal of high-rise buildings in the period 1960-1994.

From an economic standpoint, the framework reveals that losses due to the design earthquake (475 years return period) are in the range of 4,149 M€ and 13,085 M€ (5% and 95% percentile), with a median value of 9,376 M€. That is: 32,612 € per household, 17,664€ per capita. In other words, repairing the housing stock would cost an average 33% of the initial investment in building construction.

Although the most vulnerable typology are pre-code buildings (extensive damage and losses in the range 40-80%), the greatest economic bill is due to seismic damage to moderate-code and high-code RC buildings, with 75% of the total repair costs. This issue

could be explained because moderate-code and high-code gross floor area represents the 40% and 42% of the total gross floor area in the metropolitan area. The most remarkable improvement in seismic performance is related to provisions in the 1970s codes, while the current code seems more effective at reducing repair costs to short-period structures.

In this case study, the first urban expansion with RC buildings combines the highest buildability and also the greatest economic loss. In other municipalities the areas where economic losses concentrate is the urban centre, where the most ancient buildings are located and where most damage is widespread. The framework points out well delimited urban areas where economic losses concentrate, due to an unlucky combination of vulnerable buildings and high buildability or due to the building age.

In sum, the framework performs at detecting the urban areas and building typologies that should concern policymakers and researchers and provides reasonable estimates of seismic losses and damage. In comparison to other methods that hinge on tens of subjective modifiers, the proposed framework is highly automated and seems to capture more detail. Nonetheless, results from the assessment shouldn't be taken as a realistic scenario, but rather as a tool to classify buildings based on their likely seismic performance, and to translate performance into variables that can drive further decisions to assess and mitigate seismic losses.

Acknowledgements

This research is funded by (I) FEDER/Junta de Andalucía-Conserjería de Economía y Conocimiento, grant number B-TEP-306-UGR18; (II) Grant PID2020-120135RB-I00 funded by MCIN/AEI/ 10.13039/501100011033 and by the "European Union". The first author thanks the Ministry of Education for his 'Colaboración' grant.

Declaration of interest statement

The authors have no interests to declare.

References

American Society of Civil Engineers ASCE (2000). Prestandard and commentary for the seismic rehabilitation of buildings. Report FEMA 356.

Applied Technology Council (1996). Seismic evaluation and retrofit of concrete buildings. Report ATC 40.

Applied Technology Council (1985). ATC-13-Earthquake Damage Evaluation Data for California. Redwood City, California, 1985.

Applied Technology Council (1995). ATC-21-T Rapid Visual Screening of Buildings for Potential Seismic Hazards Training Manual. Redwood City, California, 1996.

Applied Technology Council (2018) FEMA P-58-3. Seismic Performance Assessment of Buildings. Volume 3 - Supporting Electronic Materials and Background Documentation. Third edition. Redwood City, California.

Applied Technology Council (2018) FEMA P-58-4. Seismic Performance Assessment of Buildings. Volume 4 - Methodology for Assessing Environmental Impacts. Redwood City, California.

Borzi, B., Dell'Acqua, F., Faravelli, M., Gamba, P., Lisini, G., Onida, M., and Polli, D. (2011). Vulnerability study on a large industrial area using satellite remotely sensed images. Bulletin of Earthquake Engineering, 9(2), 675-690.

Cabal Ramón Álvarez, Cuaresma Eduardo Díaz-Pavón, & Escribano Raúl Rodríguez. (2013). *El Terremoto de Lorca: Efectos en los edificios*. Consorcio de Compensación de Seguros.

Calvi, G. M., Priestley, M. J. N., and Kowalsky, M. J. (2007). Displacement–based seismic design of structures. Earthquake spectra, 24(2), 1-24. DOI: 10.1193/1.2932170

Chacon, J., Irigaray, C., El Hamdouni, R., Valverde-Palacios, I., Valverde-Espinosa, I., Calvo, F., ... & Lamas, F. (2012). Engineering and environmental geology of

Granada and its metropolitan area (Spain). *Environmental & Engineering Geoscience*, *18*(3), 217-260. DOI: 10.2113/gseegeosci.18.3.217

Chopra, A. K., and Goel, R. K. (1999). Capacity-demand-diagram methods based on inelastic design spectrum. Earthquake spectra, 15(4), 637-656. DOI: 10.1193/1.1586065

Cimellaro, G. P., Reinhorn, A. M., and Bruneau, M. (2010). Framework for analytical quantification of disaster resilience. Engineering structures, 32(11), 3639-3649. DOI: 10.1016/j.engstruct.2010.08.008

Directive INSPIRE (2007). Directive (Vol. 50). Directive 2007/2/EC of the European Parliament and of the Council of 14 March 2007. Official Journal of the European Union, L 108/1.

European Commission Joint Research Centre (2014) INSPIRE Thematic Working Group Cadastral Parcels. D2.8.I.6 Data Specification on Cadastral Parcels–Technical Guidelines.

European Committee for Standardization (CEN) EN 1998-1 (2004): Eurocode 8: Design of structures for earthquake resistance – Part 1: General rules, seismic actions and rules for buildings. The European Union Per Regulation 305/2011, Directive 98/34/EC, Directive2004/18/EC.

Fajfar, P., and Gašperšič, P. (1996). The N2 method for the seismic damage analysis of RC buildings. Earthquake engineering & structural dynamics, 25(1), 31-46. DOI: 10.1002/(SICI)1096-9845(199601)25:1%3C31::AID-EQE534%3E3.0.CO;2-V

Fardis, M. N. (2009). Seismic design, assessment and retrofitting of concrete buildings: based on EN-Eurocode 8 (Vol. 8). Springer Science & Business Media. DOI 10.1007/978-1-4020-9842-0

Federal Emergency Agency (2005). Report FEMA-440, Improvement of nonlinear static seismic analysis procedures. FEMA-440, Redwood City, 7(9), 11.

Federal emergency management agency (2018). Hazus-MH 2.1 Multi-hazard Loss Estimation Methodology. Earthquake Model. Technical Manual.

Feriche Fernández Castanys, Mercedes. Elaboración de escenarios de daños sísmicos en la Ciudad de Granada. Granada: Universidad de Granada, 2013. http://hdl.handle.net/10481/29803

Ferreira, T.M., Maio, R., and Vicente, R. Seismic vulnerability assessment of the old city centre of Horta, Azores: calibration and application of a seismic vulnerability index method. Bull Earthquake Eng 15, 2879–2899 (2017). https://doi.org/10.1007/s10518-016-0071-9

Flores, K.L., Escudero, C.R., and Zamora-Camacho, A. Multicriteria seismic hazard assessment in Puerto Vallarta metropolitan area, Mexico. Nat Hazards 105, 253–275 (2021). https://doi.org/10.1007/s11069-020-04308-x

Freeman, S. A. (1998, September). The capacity spectrum method. In Proceedings of the 11th European conference on earthquake engineering, Paris.

Gentile, R., & Galasso, C. (2020). Gaussian process regression for seismic fragility assessment of building portfolios. Structural Safety, 87, 101980. DOI: 10.1016/j.strusafe.2020.101980

Gonzalez, D., Rueda-Plata, D., Acevedo, A. B., Duque, J. C., Ramos-Pollán, R., Betancourt, A., and García, S. (2020). Automatic detection of building typology using deep learning methods on street level images. Building and Environment, 106805. DOI: 10.1016/j.buildenv.2020.106805

Hashemi, M., and Alesheikh, A. A. (2011). A GIS-based earthquake damage assessment and settlement methodology. Soil dynamics and earthquake engineering, 31(11), 1607-1617.

Kappos, A. J., Panagopoulos, G., Panagiotopoulos, C., and Penelis, G. (2006). A hybrid method for the vulnerability assessment of R/C and URM buildings. Bulletin of Earthquake Engineering, 4(4), 391-413. DOI: 10.1007/s10518-006-9023-0

Karimzadeh, S., Miyajima, M., Hassanzadeh, R., Amiraslanzadeh, R., and Kamel, B. (2014). A GIS-based seismic hazard, building vulnerability and human loss assessment for the earthquake scenario in Tabriz. Soil Dynamics and Earthquake Engineering, 66, 263-280.

Kim, H. S., Sun, C. G., Kim, M., Cho, H. I., and Lee, M. G. (2020). GIS-Based Optimum Geospatial Characterization for Seismic Site Effect Assessment in an Inland Urban Area, South Korea. Applied Sciences, 10(21), 7443. https://doi.org/10.3390/app10217443

Kircher, C. A., Whitman, R. V., and Holmes, W. T. (2006). HAZUS earthquake loss estimation methods. Natural Hazards Review, 7(2), 45-59. DOI: 10.1061/(ASCE)1527-6988(2006)7:2(45)

Lantada, N., Irizarry, J., Barbat, A. H., Goula, X., Roca, A., Susagna, T., and Pujades, L. G. (2010). Seismic hazard and risk scenarios for Barcelona, Spain, using the Risk-UE vulnerability index method. Bulletin of earthquake engineering, 8(2), 201-229. DOI: 10.1007/s10518-009-9148-z

Liu, Y., So, E., Li, Z., Su, G., Gross, L., Li, X., Qi, W., Yang, F., Fu, B., Yalikun, A., et al. (2020). Scenario-based seismic vulnerability and hazard analyses to help direct disaster risk reduction in rural Weinan, China. International Journal of Disaster Risk Reduction, 48, 101577.

McCormack, T. C., and Rad, F. N. (1997). An earthquake loss estimation methodology for buildings based on ATC-13 and ATC-21. Earthquake Spectra, 13(4), 605-621. DOI: 10.1193/1.1585971

McKinney, W. (2015). Pandas, python data analysis library http://pandas.pydata.org

Ministerio de Fomento (2002). Norma de construcción sismorresistente: parte general y edificación (NCSR-02). BOE-A-2002-19687. BOE núm 244, 11/11/2002, pp. 35898-35967. https://www.boe.es/eli/es/rd/2002/09/27/997

Ministerio de Obras Públicas, Transportes y Medio Ambiente (1994). Construcción Sismorresistente: Parte General y Edificación (NCSE-94). BOE-A-1995-3319. BOE núm 33, 08/02/1995, pp 3935-3980. https://www.boe.es/eli/es/rd/1994/12/29/2543

Ministerio de Planificación del Desarrollo (1974). Norma Sismorresistente P.D.S-1 parta A. BOE-A-1974-1869. BOE núm. 279, 21/11/1974, pp 23585-23601.

Ministerio de Vivienda (1963). Norma MV-101/1962 Acciones en la Edificación. BOE-A-1963-4613. BOE núm. 35, 09/02/1963, pp 2207-2225.

Montilla, J. A. P., de Galdeano, C. S., and Casado, C. L. (2003). Use of active fault data versus Seismicity data in the Evaluation of seismic Hazard in the Granada basin (Southern Spain). Bulletin of the Seismological Society of America, 93(4), 1670-1678. DOI: 10.1785/0120020110

Mouroux, P., and Le Brun, B. (2006). Presentation of RISK-UE project. Bulletin of Earthquake Engineering, 4(4), 323-339. DOI: 10.1007/s10518-006-9020-3

Presidencia del Gobierno (1968). Norma sismorresistente PGS 1 Parte A. BOE-A-1969-148. BOE núm. 30, 04/02/1969, pp 1658-1675.

QGIS.org, 2021. QGIS Geographic Information System. QGIS Association. http://www.qgis.org

Quinay, P. E. B., Soliman, J. M. M., and Fader, A. R. F. (2020). Development of Simulation-Based Approach Using Frame Models Generated From GIS Features and BIM Data for Application to City Seismic Response Analysis of Low-to Mid-Rise RC Structures in Metro Manila. Journal of Earthquake and Tsunami, 14(06), 2050021.

RADIUS (1999) Risk Assessment Tools for Diagnosis of Urban Areas Against Seismic Disasters. Cities involved: Tijuana-Mexico, Guyaquil-Ecuador, Antofagasta-Chile, Skopje-FYROM, Izmir-Turkey, Addis Ababa-Ethiopia, Tachkent-Ouzbekistan, Bandung-Indonesia, Zigong-China. Report: United Nations initiative towards Earthquake Safe Cities.

Rajarathnam, S., and Santhakumar, A. R. (2015). Assessment of seismic building vulnerability based on rapid visual screening technique aided by aerial photographs on a GIS platform. Natural Hazards, 78(2), 779-802. DOI: 10.1007/s11069-014-1382-2

Riaño, A. C., Reyes, J. C., Yamín, L. E., Bielak, J., Taborda, R., and Restrepo, D. (2021). Integration of 3D large-scale earthquake simulations into the assessment of the seismic risk of Bogota, Colombia. Earthquake Engineering & Structural Dynamics, 50(1), 155-176. DOI: 10.1002/eqe.3373

Riedel, I., Guéguen, P., Dalla Mura, M., Pathier, E., Leduc, T., and Chanussot, J. Seismic vulnerability assessment of urban environments in moderate-to-low seismic hazard regions using association rule learning and support vector machine methods. Nat Hazards 76, 1111–1141 (2015). https://doi.org/10.1007/s11069-014-1538-0

SEAOC Seismology Committee. (2006). SEAOC Blue Book: Seismic Design Recommendations. Structural Engineers Association of California, Sacramento, CA.

Torres, Y., Arranz, J. J., Gaspar-Escribano, J. M., Haghi, A., Martínez-Cuevas, S., Benito, B., and Ojeda, J. C. (2019). Integration of LiDAR and multispectral images for rapid exposure and earthquake vulnerability estimation. Application in Lorca, Spain. International Journal of Applied Earth Observation and Geoinformation, 81, 161-175.

Van Loenen, B., and Grothe, M. (2014). INSPIRE empowers re-use of public sector information. International Journal of Spatial Data Infrastructures Research, 9, 96-106. DOI: 10.2902/1725-0463.2014.09.art4

Valverde-Palacios, I. (2010). Cimentaciones de edificios en condiciones estáticas y dinámicas: casos de estudio al W de la ciudad de Granada. Universidad de Granada. http://hdl.handle.net/10481/5636

Valverde-Palacios, I., Valverde-Espinosa, I., Irigaray, C., & Chacón, J. (2014). Geotechnical map of Holocene alluvial soil deposits in the metropolitan area of Granada (Spain): a GIS approach. *Bulletin of Engineering Geology and the Environment*, *73*(1), 177-192. DOI: 10.1007/s10064-013-0540-1

Appendix A

This appendix shows a diagram with the workflow of the framework (Fig. A1) and all the parameters involved in the calculations of the sample building in Fig. 2 are shown in Table A1 and A2.

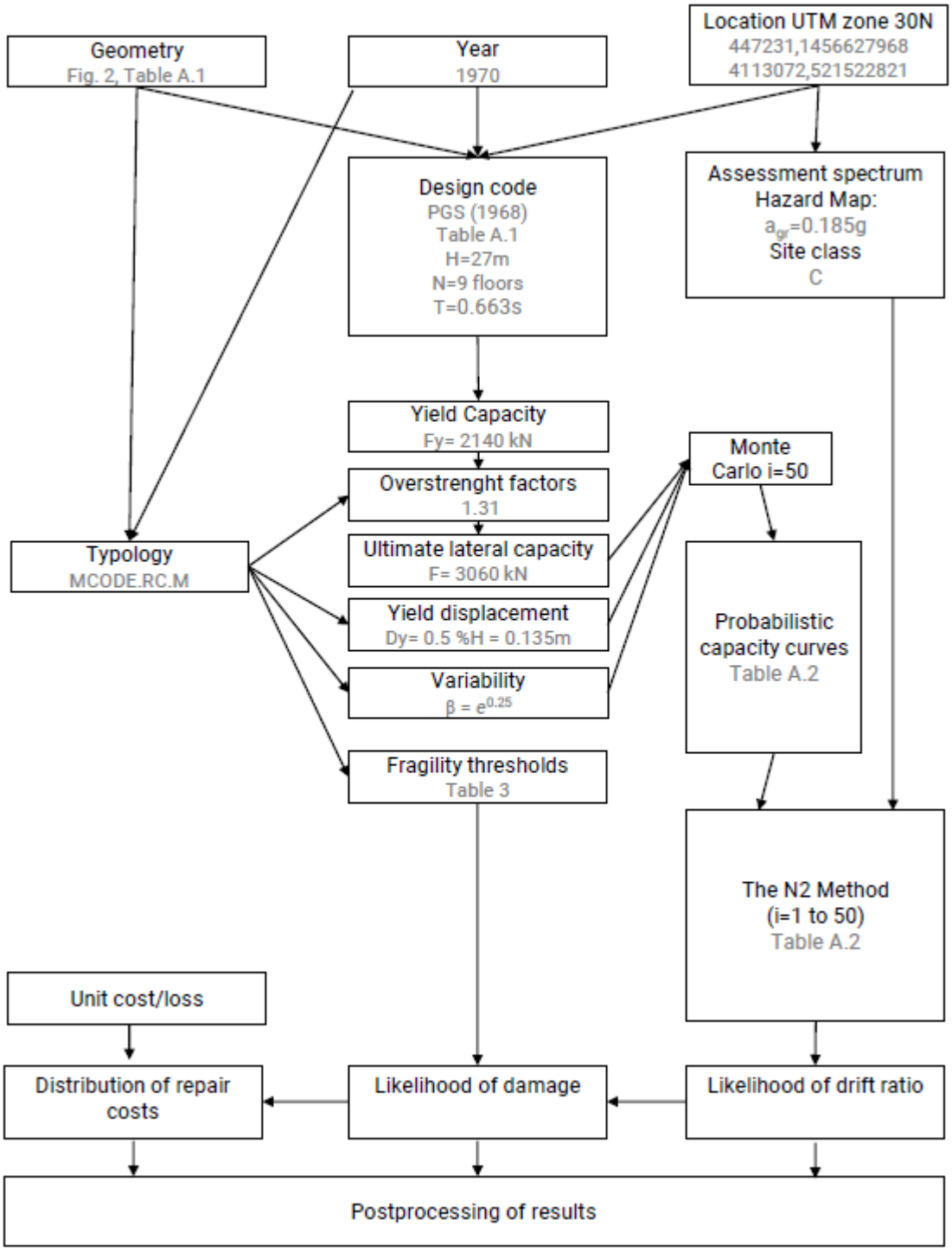

Fig. A1: Workflow of the proposed assessment framework

Table A1. Parameters of sample building: Cadastral attributes, design code calculations, representative the capacity curve, and assessment spectrum.

Parameter	Value	Units
Location	37.162502212868205, -3.5944272679164606	WGS 84 Web Mercator
Building cadastral ID	7433601VG4173C	
Current use	1_residential	
Number of dwellings	27	dwellings
Total gross area	3053	m^2
Year	1970	
Max number of floors	9	
Smaller building side length	13.42	m
Surface vector	[321 305 205 305 305 305 305 276 23]	m^2
Height vector [H]	[3 6 9 12 15 18 21 24 27]	m
Mass vector [m]	[256800. 244000. 244000. 244000. 244000. 244000. 244000. 213600. 18400.]	kg
Total weight	1952800	kg
Construction cost	600	€/m2
Typology	MCODE.RC.H	
Code	PGS-1 (1968)	
Period in the design code	0.663	s
c (design value)	0.131964354	
$\gamma_1 \cdot \gamma_2$	1.43	
c	0.188709026	
Dy	0.135	m
[ϕ1]	[0.173, 0.342, 0.500, 0.642, 0.766 0.866, 0.939 , 0.984 , 1.000]	
L_1	1263150.92	kg
M_1	965302.64	kg
Γ_1	1.31	
$M_{eff,1}$	1652901.57	kg
Fy	2139797.30	N
F (representative value)	3059910.14	N
Variability (Beta)	1.284025	
EC8_ground type	C	
Factor K Azores seismicity	1	
$v_{s,30}$	330	m/s
$a_{g,r}$ @ stiff rock	1.81	m/s^2
EC8 factor C	1.51	
Soil amplification factor S	1.37	
a_{gr}*S	2.47	m/s^2
T_b	0.08	s
T_c	0.38	s
T_d	2.00	s

Table A2. Parameters of the sample building: Probabilistic capacity curves, N2 method calculation, performance point, damage states and repair costs.

i	T^* (s)	S_e (m/s^2)	F^* (kN)	d^*_y(m)	d (m)	d (%H)	DS	Repair cost (€)
1	1.60	3.05	3238	0.166	0.258	0.96	2	696084
2	1.73	2.81	2477	0.149	0.280	1.04	2	696084
3	1.18	4.15	4382	0.121	0.190	0.70	2	696084
4	1.48	3.29	4008	0.176	0.239	0.89	2	696084
5	1.71	2.84	2346	0.138	0.277	1.03	2	696084
6	1.52	3.21	3027	0.140	0.246	0.91	2	696084
7	2.47	3.94	1462	0.179	0.800	2.96	3	1392168
8	1.03	4.73	4439	0.095	0.167	0.62	2	696084
9	1.84	2.65	2460	0.167	0.298	1.10	2	696084
10	1.44	3.39	4382	0.182	0.233	0.86	2	696084
11	1.29	3.77	3689	0.124	0.209	0.77	2	696084
12	1.98	2.46	2333	0.184	0.320	1.19	3	1392168
13	1.50	3.25	2710	0.122	0.243	0.90	2	696084
14	1.87	2.61	2116	0.148	0.302	1.12	2	696084
15	1.74	2.80	1868	0.113	0.281	1.04	2	696084
16	1.29	3.78	3311	0.111	0.209	0.77	2	696084
17	1.06	4.60	3816	0.086	0.171	0.63	2	696084
18	1.09	4.45	3639	0.087	0.177	0.66	2	696084
19	1.61	3.03	3510	0.182	0.260	0.96	2	696084
20	1.36	3.58	2837	0.105	0.220	0.81	2	696084
21	1.44	3.39	3613	0.150	0.233	0.86	2	696084
22	1.87	2.61	2237	0.157	0.302	1.12	2	696084
23	1.10	4.43	3980	0.097	0.178	0.66	2	696084
24	1.95	2.50	3022	0.231	0.316	1.17	2	696084
25	1.35	3.61	2443	0.089	0.218	0.81	2	696084
26	1.81	2.69	1880	0.124	0.293	1.08	2	696084
27	1.57	3.10	4387	0.218	0.254	0.94	2	696084
28	1.50	3.26	2810	0.126	0.242	0.90	2	696084
29	1.74	2.81	3164	0.191	0.281	1.04	2	696084
30	1.41	3.46	3268	0.130	0.228	0.84	2	696084
31	1.50	3.24	3009	0.137	0.243	0.90	2	696084
32	1.44	3.39	3623	0.151	0.233	0.86	2	696084
33	1.29	3.77	3991	0.133	0.209	0.77	2	696084
34	1.68	2.90	2509	0.142	0.272	1.01	2	696084
35	1.29	3.76	3230	0.109	0.209	0.78	2	696084
36	1.70	2.87	2451	0.142	0.275	1.02	2	696084
37	1.23	3.97	3363	0.101	0.198	0.73	2	696084
38	2.42	4.03	1536	0.180	0.782	2.89	3	1392168
39	1.52	3.21	2913	0.135	0.246	0.91	2	696084
40	1.90	2.57	1982	0.143	0.307	1.14	2	696084
41	1.57	3.11	4474	0.221	0.254	0.94	2	696084
42	2.08	4.68	1682	0.146	0.674	2.49	3	1392168
43	1.22	4.01	4472	0.133	0.197	0.73	2	696084
44	1.96	2.49	1830	0.141	0.317	1.17	3	1392168
45	1.73	2.81	2668	0.161	0.280	1.04	2	696084
46	1.49	3.26	3483	0.156	0.242	0.89	2	696084
47	1.07	4.54	4175	0.097	0.174	0.64	2	696084
48	1.57	3.10	3019	0.150	0.255	0.94	2	696084
49	1.32	3.68	4446	0.156	0.214	0.79	2	696084
50	2.01	4.85	1413	0.115	0.650	2.41	3	1392168
μ	1.57	3.41	3062.46	0.14	0.28	1.05	2.12	779614
σ	0.33	0.66	895.08	0.03	0.14	0.52	0.33	228497
σ/ μ	20.84	19.46	29.23	24.04	49.25	49.24	15.48	29.31

μ = average value; σ = standard deviation, σ/ μ = coefficient of variation (%)

Table 1. Sample of the attributes in the geospatial database for the example building.

Cadastral Reference	Use	Year	Gross floor area (m^2)
7433601VG4173C	Residential	1970	3053

	Vol_1	Vol_2	Vol_3	Vol_4	Vol_5	Vol_6	Vol_7	Vol_8
Number of floors	9	2	2	10	8	8	8	8
Area (m^2)	272	4	14	24	12	8	17	4

Table 2. Parameters related to the building's categories.

Code	Description	Year	Floors	γ_1	γ_2	β	D_y
PCODE.MA.L	Masonry low-rise precode building	Before 1956	[1, 2]	1.5	3	0.3	0.25
PCODE.MA.M	Masonry medium-rise precode building	Before 1956	[3, 5]	1.25	3	0.3	0.25
PCODE.MA.H	Masonry high-rise precode building	Before 1956	[6, 9]	1.1	3	0.3	0.25
PCODE.RC.M	RC medium-rise precode building	[1956, 1968]	[3, 7]	1.25	2	0.3	0.5
PCODE.RC.H	RC high-rise precode building	[1956, 1968]	[8, 12]	1.1	2	0.3	0.5
MCODE.RC.L	RC low-rise moderate code building	[1969, 1994]	[1, 3]	1.5	1.3	0.25	0.5
MCODE.RC.M	RC medium-rise moderate code building	[1969, 1994]	[4, 7]	1.25	1.3	0.25	0.5
MCODE.RC.H	RC high-rise moderate code building	[1969, 1994]	[8, 13]	1.1	1.3	0.25	0.5
HCODE.RC.L	RC low-rise highcode building	[1994, 2019]	[1, 3]	1.25	1.3	0.25	0.5
HCODE.RC.M	RC medium-rise highcode building	[1994, 2019]	[4, 7]	1.25	1.3	0.25	0.5
HCODE.RC.H	RC high-rise highcode building	[1994, 2019]	[8, 12]	1.1	1.3	0.25	0.5

Table 3. Lateral displacement thresholds as percentage of the building height and corresponding damage states

Class	DS_1	DS_2	DS_3	DS_4
PCODE.MA.L	0.0032	0.0051	0.0128	0.0350
PCODE.MA.M	0.0021	0.0034	0.0086	0.0233
PCODE.MA.H	0.0016	0.0026	0.0064	0.0175
PCODE.RC.M	0.0027	0.0043	0.0107	0.0267
PCODE.RC.H	0.0020	0.0032	0.0080	0.0200
MCODE.RC.L	0.0050	0.0087	0.0233	0.0600
MCODE.RC.M	0.0033	0.0058	0.0156	0.0400
MCODE.RC.H	0.0025	0.0043	0.0117	0.0300
HCODE.RC.L	0.0050	0.0100	0.0300	0.0800
HCODE.RC.M	0.0033	0.0067	0.0200	0.0533
HCODE.RC.H	0.0025	0.005	0.0150	0.0400

Figure captions

Fig. 1: Steps in methodology.

Fig. 2: Sample of the vector data in the geospatial database.

Fig. 2(a): Example building.

Fig. 2(b): Vector data.

Fig 3: Example of classification algorithm.

Fig. 4: Capacity curves.

Fig4(a): Idealisation of a capacity curve.

Fig4(b): Probabilistic capacity curve.

Fig. 5: Probability distribution of drift ratios in an example building.

Fig. 6: Maps of Granada Metropolitan Area

Fig. 6(a): Andalucía 475-year return period hazard map

Fig 6(b): Urban areas

Fig.7: Evolution of the housing gross floor area in the Metropolitan area of Granada.

Fig. 8: Design response spectra in Spanish building codes MV101, PDS1, NCSE-02 with different values of the behaviour factor q.

Fig. 9: Distribution of story height and: (a) number of floors, (b) seismic code.

Fig. 10: Sample map of building categories in the metropolitan area of Granada.

Fig. 11: Elastic seismic response spectra for ground type C (Vs=330 m/s).

Figure 12: Sample map of median target displacements as a percentage of the building height.

Fig. 13: Representative seismic damage under different seismic codes.

Fig.14: Sample maps of representative seismic damage.

Fig. 15: Histograms of seismic damage.

Fig. 15(a): By building category.

Fig. 15(b): By number of stories.